Hydrogen and deuterium diffusion in non-stoichiometric spinel

Link:
Link to publication record in Edinburgh Research Explorer

Document Version:
Publisher's PDF, also known as Version of record

Published In:
High Pressure Research

Hydrogen and deuterium diffusion in non-stoichiometric spinel

Geoffrey D. Bromiley , Jennifer Brooke & Simon C. Kohn

Published online: 12 Jul 2017.

Submit your article to this journal ⏎

Article views: 71

View related articles ⏎

View Crossmark data ⏎

Taylor & Francis
Taylor & Francis Group

ᵃ OPEN ACCESS Check for updates

Hydrogen and deuterium diffusion in non-stoichiometric spinel

Geoffrey D. Bromiley [a,b], Jennifer Brooke[a] and Simon C. Kohn[c]

[a]School of GeoSciences, University of Edinburgh, King's Buildings, Edinburgh, UK; [b]Centre for Science at Extreme Conditions, Erskine Williamson Building, King's Buildings, Edinburgh, UK; [c]School of Earth Sciences, Will's Memorial Building, Bristol, UK

ABSTRACT
High pressure/temperature annealing experiments are used to determine diffusivities of H^+ and D^+ in non-stoichiometric spinel, a low-pressure analogue for nominally anhydrous minerals in Earth's mantle. Data are fitted to the following Arrhenius law: Diffusivity $(m^2/s) = 4 \pm 1 \times 10^{-12} \exp(-54 \pm 2 \text{ kJ mol}^{-1}/RT)$. At low temperatures, H^+ and D^+ diffusion in non-stoichiometric spinel is charge balanced by flux of O vacancies, with infrared data consistent with protonation of both octahedral and tetrahedral O–O edges in non-stoichiometric spinel, and additional fine structure due to Mg–Al mixing and/or coupling of structurally incorporated H^+ with cation vacancies. Absence of changes in the fine structure of O–H absorption bands indicates that H^+ can become locally coupled and uncoupled to other defects during bulk diffusion. As such, proton conductivity in spinel group minerals, arising from faster flux of uncoupled H^+, can only be calculated from H^+ mobility data if the extent of defect coupling is constrained.

Introduction

The nominally anhydrous minerals (NAMs) which constitute the silicate mantles of Earth and terrestrial planets can incorporate significant quantities of dissolved 'water' in the form of structurally incorporated hydrogen (H^+). This H^+ is typically bound to relatively underbonded oxygens, forming spectroscopically active hydroxyl (OH^-) groups, often associated with other defects such as cation vacancies [1,2]. The corresponding hydroxyl solubility in NAMs varies from a few tens to tens of thousands of ppm H_2O by weight (parts per million H_2O by weight (ppmw)), and represents a highly efficient mechanism for storing considerable quantities of water in Earth's deep interior, comparable to the volume of water present in the hydrosphere [3]. The presence of H^+ also has important influences on a range of mineral and bulk mantle properties, such as melting behaviour, electrical conductivity, seismic velocities and rheology [4–8].

Spinel sensu stricto, $MgAl_2O_4$, is volumetrically a minor phase in the upper part of the Earth's mantle and the main repository for Al to depths of 50–80 km, and can only incorporate trace amounts of hydoxyl [9]. However, Bromiley et al. [10] demonstrated that synthetic, non-stoichiometric, Al-rich spinel can incorporate significant quantities of hydroxyl under high pressure/temperature (HPT) (P–T) mantle conditions, and may provide a useful, low-pressure analogue for detailed investigations of H incorporation in NAMs. In particular, large gem-quality crystals of non-stoichiometric spinel can be readily synthesised, enabling detailed studies of H^+ incorporation mechanisms and defect coupling using multiple techniques, something which is challenging to perform on run products from high PT studies of mantle minerals. Non-stoichiometric spinel is isostructural with ringwoodite, $(Fe,Mg)_2SiO_4$, the main mineral stable in the lower part of Earth's transition zone, and a phase believed to incorporate significant volumes of water (*i.e.* hydroxyl) in the deep Earth [3,11–13]. In addition to the insight which it provides on H^+ incorporation in major mantle NAMs, non-stoichiometric spinel has several potential technological applications, most notably as a proton conductor and H^+ sensor, and has been the subject of numerous investigations of electrochemical properties [14–16].

Spinel sensu stricto and ringwoodite are both minerals within the spinel mineral class. Spinel class minerals have the general formula XY_2O_4, in which X and Y are divalent, trivalent, or quadrivalent cations. The structure can be described as an ideal cubic close-packed array of O anions in which cations occupy 1/8 of the tetrahedral and ½ of the octahedral interstices. In an ideal fully ordered spinel T (tetrahedral) sites and M (octahedral) sites are occupied by X and Y cations, respectively, although in practice, spinel group minerals are characterised by varying degrees of cation disorder and mixing of X and Y over both sites, especially at elevated temperature [17]. In fully ordered, stoichiometric spinel, $MgAl_2O_4$ ('ideal spinel'), Mg fully occupies T sites and Al fully occupies M sites. Bromiley et al. [10] demonstrated that non-stoichiometric spinel contains a significant proportion of both Al-occupied T sites and vacant M sites, resulting in a structure with an H^+ solubility several orders of magnitude higher than ideal spinel. However, although Bromiley et al. [10] performed a series of high PT annealing experiments on non-stoichiometric spinel, problems with recrystallisation (due to the inherent instability of non-stoichiometric spinel at high temperature) prevented them from extracting key data on H diffusivity during annealing. Assessing H mobility in NAMs is essential in constraining the importance of H^+ incorporation on mantle properties and processes within the deep Earth, and in providing additional insight into H^+ incorporation mechanisms, for example [18–21]. H^+ mobility in non-stoichiometric spinel has been investigated by Canova et al. [22], Fukatsu et al. [14] and Gonzalez et al. [16], although these studies provide only limited insight into the relative mobility of different H^+ defects. Furthermore, these studies were performed by annealing non-stoichiometric spinel in H-rich atmospheres at ambient pressure, and not at the high P–T conditions under which it can incorporate quantities of H^+ comparable to other mantle NAMs. The purpose of this study is to conduct high PT experiments to determine both H^+ and D^+ diffusivity in non-stoichiometric spinel coupled with high-resolution spectroscopic examination of H incorporation mechanisms.

Methods

Starting material and HPT annealing

The starting material for this study was a non-stoichiometric spinel from the same batch used in hydration experiments by Bromiley et al. [10] (their sample 'synthetic spinel 1'), synthesised at ambient pressure and high temperature from spec-pure reagents using the Verneuil method. Pieces of this material were prepared as $1 \times 1 \times 2$ mm polished rectangular prisms, cut using a diamond wire saw and polished gently using up to 1 μm diamond polishing suspensions. Composition of the material, as determined by electron microprobe (EMP) (details in Section 2.2) is as follows: Mg: 6.62(5)%, Al: 47.43(14)%, O: 47.52(15), where values are averaged element weight percent, and values in parentheses are standard deviations on the last figure for averaged compositions. No B was detected in the sample during analysis (detection limit 150–200 ppmw), and the fact that it is colourless implies no contamination due to the presence of even trace amounts of transition metals such as Fe and Cr. Single crystal X-ray data [10] demonstrates that this synthetic spinel has excess Al_2O_3, resulting in T site contraction, and a significantly increased M site volume due to the presence of a significant proportion of cation vacancies.

Prepared cuboids of the spinel were loaded into 2 mm diameter Pt capsules, along with a high-purity non-stoichiometric mix of Al_2O_3 and MgO (with the same composition as the spinel) and 10 wt% distilled H_2O or high-purity D_2O. Capsules were then welded shut and checked for leaks. For each HPT annealing experiment, one H_2O and one D_2O-bearing capsule were prepared. Both capsules were loaded side by side in an alumina sample holder, and then inserted into a 0.75′ talc-pyrex-graphite piston-cylinder assembly, as described in [23] and shown in Figure 1. Piston-cylinder experiments were run using the 'hot-piston out technique', in which pressure was slowly ramped to 110% of the final run pressure (1 GPa in all experiments), and temperature then slowly ramped to the final run temperature whilst maintaining pressure. Pressure was then slowly released by bleeding off hydraulic fluid until the desired pressure was reached. Pressure and temperature were monitored and maintained throughout the duration of experiments. Temperatures were measured using a type R thermocouple, with the thermocouple junction placed within 0.5 mm of the end of the Pt capsules, separated by a thin alumina disc. Use of tapered graphite furnaces minimises thermal gradients across the capsules, which are <10°C from hot spot, located towards the upper part of the sample volume, to the lower edge of the sample volume, under the run conditions used here (Bromiley, unpublished data). Experiments were quenched by switching off power to the heating circuit, resulting in rapid quenching (temperatures fell to below 100°C within 15 s), followed by room temperature decompression over approximately 1 hour. Run conditions and results are listed in Table 1. After all experiments, both capsules were carefully recovered and examined, although recrystallisation of alumina around capsules prevented accurate weighing to check for the presence of water after the experiments. Recovered annealed samples were sectioned using a 0.2 mm diamond wire saw to produce a thin slice of spinel from the central portion of the cuboid, as shown in Figure 1. Slices were then polished to produce double-polished plates using standard diamond polishing solutions. During preparation, spinel samples and slices were mounted and bonded using Crystalbond™. At each stage of preparation, and after the final stage of preparation of doubly polished sections, all
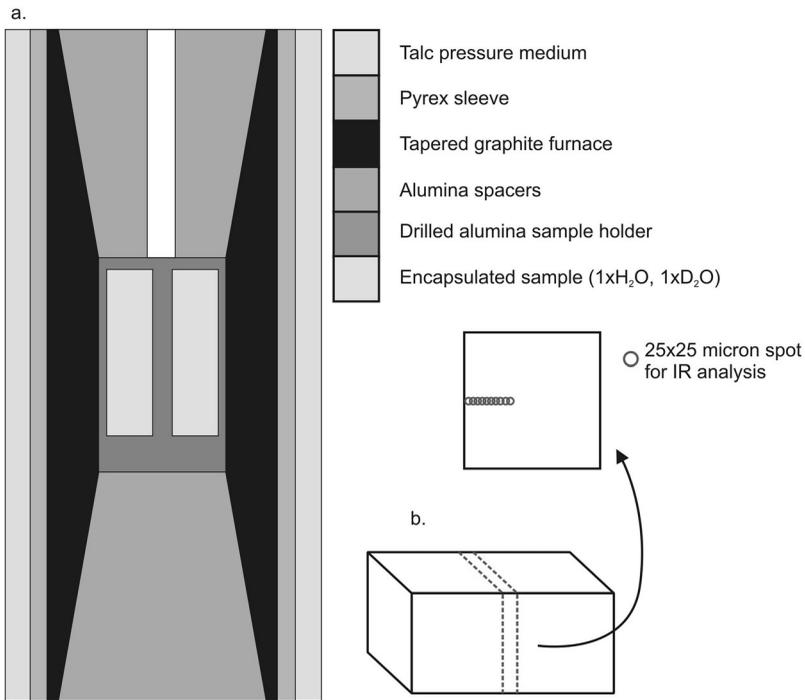
Figure 1. Experimental setup used for spinel diffusion experiments. (a) 0.75′ piston-cylinder assembly with tapered furnace used to reduce thermal gradients in sample volume. Two capsules were loaded into both assemblies, one saturated in H_2O, the other saturated in D_2O. (b) Sketch showing spinel crystal ($2 \times 1 \times 1$ mm) cuboids loaded into each capsule. Recovered cuboids were then cut as shown (dashed red line) using a diamond wire saw to produce a slice across the central region. Slices were polished down to 1 μm using diamond pastes. IR spectra were then obtained from the edge of slices inwards to determine 1-D diffusion profiles, as shown.

traces of Crystalbond™ were removed by repeatedly soaking samples in high-purity acetone for up to 24 hours, before gently wiping with high-purity ethanol using lint-free tissue to remove any residues. After infrared (IR) analysis had been performed, polished sections were then remounted in epoxy and polished for EMP analysis.

Table 1. Run conditions and results for non-stoichiometric spinel experiments.

Experiment	Temp (K)	Time (h)	Sample	Notes
Hysp1	673	97	H_2O	Spinel completely recrystallised; hydrous phase(s) formed?
			D_2O	Spinel completely recrystallised; hydrous phase(s) formed?
Hysp5	773	97.5	H_2O	H loss from samples resulting in diffusion gradient
			D_2O	No O–D detected; H loss from samples resulting in diffusion gradient
Hysp3	873	75	H_2O	H diffusion into the sample resulting in concentration gradient
			D_2O	No O–D detected; H loss from samples resulting in a concentration gradient
Hysp6	973	47	H_2O	H loss from samples resulting in concentration gradient
			D_2O	D and H diffusion into sample
Hysp4	1073	41	H_2O	H diffusion into the sample resulting in concentration gradient
			D_2O	No O–D detected; H loss from samples resulting in a concentration gradient

Notes: Two capsules were prepared for each experiment, one H_2O bearing, the other D_2O bearing. Pressure was 1 GPa for all annealing experiments.

Sample analysis

IR spectra were obtained along transects across prepared slices using a Thermo-Nicolet iN10MX IR microscope at the School of Earth Sciences, University of Bristol. Samples were placed on thin BaF_2 plates, and unpolarised spectra (and some additional polarised spectra) collected over the range 4000–450 cm^{-1}. Background spectra were obtained through the BaF_2 plate prior to each transect, and automatically subtracted from sample spectra. For all samples, a 25×25 μm aperture was used and spectra obtained at 20 μm steps across sample slices, from edge to centre, with positioning automatically controlled by a motorised sample stage (see Figure 1(b)). Spectral resolution was set at either 4 or 8 cm^{-1}, with mid-IR spectra obtained using an Ever-Glo™ IR source, liquid N_2-cooled MCT-A detector and using a multi-coated KBr/germanium beamsplitter. All the data presented here were obtained using unpolarised IR radiation. In addition, a few polarised spectra were taken using a ZnSe wire-grid polariser, to verify that the OH absorptions were isotropic. Spectra were thickness and background corrected (using a linear baseline over the region 4000–2500 cm^{-1}) and fitted using IGOR Pro™ software, using the Multipeak Fitting 2 toolbox.

Starting material and all annealed samples were subsequently prepared for compositional analysis by EMP. A well-characterised synthetic stoichiometric spinel standard (Spinel BLZ, University of Edinburgh) was used for analysing Mg (Kα, LTAP, 20 s count time), Al (Kα, TAP, 20 s) and O (Kα, PC1, 20 s) using a Cameca SX100 EMP with a finely focussed (approximately 1.5 μm diameter) beam running at 15 keV accelerating voltage and 10 nA current.

O–H and O–D absorption in IR spectra

Bromiley et al. [10] noted that in contrast to previous studies, complexity in the O–H absorption region for non-stoichiometric spinel could be best fitted to at least three separate O–H stretching contributions, including an absorption band at 3343–3352 cm^{-1} and a doublet consisting of two distinct O–H bands at 3505–3517 and 3557–3566 cm^{-1}. Similarly, we noted that in the majority of spectra it was clear that several contributions are needed to adequately fit IR spectra over the region due to both O–H and O–D stretching (4000–2000 cm^{-1}), and that the two main contributions in the range of stretching frequencies corresponding to O–H absorption clearly exhibit some fine structure (Figure 2). Although IR spectra consist of two distinct contributions, they cannot be adequately fitted to two single Gaussians, and residuals suggest the presence of additional contributions (Figure 2(a)). Figure 2(b) shows the result of fitting three contributions, as suggested by Bromiley et al. [10]. Although fit is improved, in particular relative to the doublet around 3500–3600 cm^{-1} residuals suggest that at least one additional contribution is required to fit the spectra, indicating that the absorption feature centred around 3300 cm^{-1} might also be a doublet. Figure 2(c) shows improvements when fitting data to four Gaussian contributions. However, no consistent method could be produced to adequately fit an additional contribution, especially in samples with lower bulk water contents, due to the extensive overlap between the four peaks, inherent problems with spectral deconvolution, and lower signal to noise ratios in some spectra. This is apparent in Figure 2(c), in which a much broader fourth contribution always results from peak
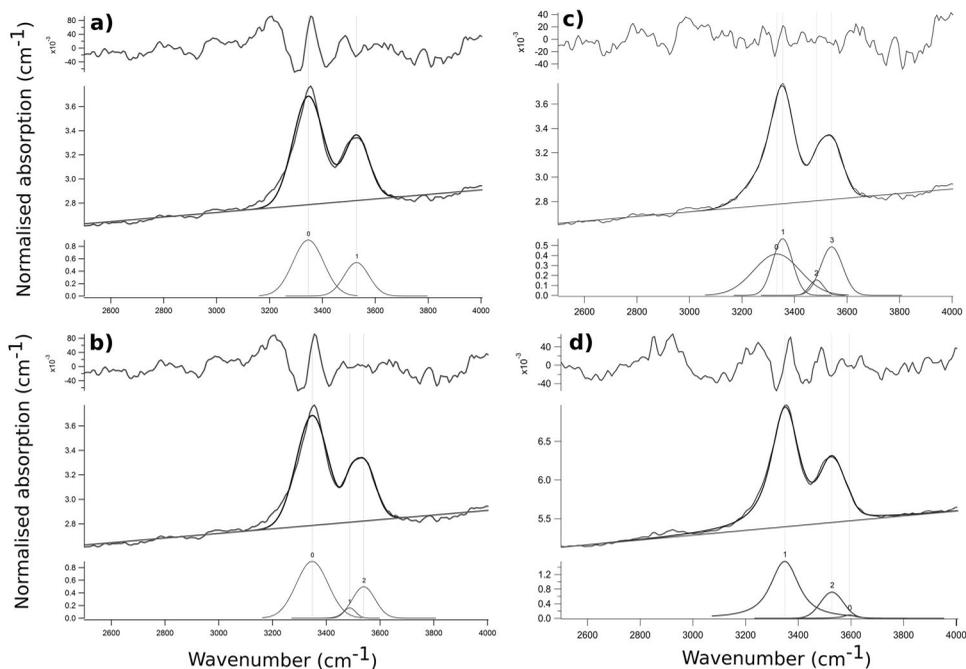
Figure 2. Examples of fitting non-stoichiometric spinel IR spectra using different numbers of contributions. (a) Fitting Gaussians to two contributions; (b) fitting three Gaussians to (three contributions, bands 1, 2a and 2b, consistent with [10]; (c) fitting four Gaussians (*i.e.* recognising splitting of both major O–H features) results in a best fit to IR data and minimises residual; (d) procedure used to consistently fit IR data across transects adopted from [10] where both O–H features are modelled with Lorentzian and Gaussian contributions, with an additional minor peak to represent splitting of OH feature 2. Whilst less accurate than (c) this procedure could be used consistently across all data. Centre part in each figure is the original IR data (grey), fitted to a linear background and to the various modelled peaks (black), with individual contributions shown in the lower part of each figure. Upper part of each figure shows residuals from fitting.

fitting. An approach of using several additional contributions to fit the typically non-linear spectral baselines was attempted, thereby increasing the overall quality of the fit. However, variations in the baselines between spectra across individual transects meant that this approach could not be used to obtain consistent, accurate, comparative data on trends in O–H absorption (*i.e.* integral of individual H–O stretching contributions in absorption spectra). Therefore, we adopted an approach similar to that used by Bromiley et al. [10], modelling the two O–H bands/regions separately using a combination of Gaussian and Lorentzian contributions to both (Figure 2(d)). This consistent approach meant that relative error between spectral fitting in each line transect was minimised.

OH contents were determined from IR data using the calibration of Libowitzky and Rossman [24] in which integrated area of O–H absorption bands is used to determine OH concentrations (in mol H_2O/L) in accordance with the Beer–Lambert law and a wavenumber-dependent generalised molar absorption coefficient for water. This provides a more accurate determination of water contents of samples than the older calibration of Paterson [25], due to its dependence on absorption in hydrous glasses containing varied hydrous species. Recalculating water contents for the non-stoichiometric spinel

starting material by Bromiley et al. [10] using the Libowitzky calibration gives excellent agreement with the present study, as would be expected, and indicates that water contents given in Bromiley et al. [10] might be overestimated by 20–30%. However, we also observed additional variations in the starting water contents of the non-stoichiometric spinel, from 10 to 40ppmw; this variability was not noted by Bromiley et al. (2010) because they studied a small quantity of material prepared from a small volume of one single boule. In this study, spinel cuboids were prepared from different boules in the same sample batch. However, within each annealed sample slice, and within unannealed sample slices, no significant variation in volatile content was noted other than diffusion profiles arising from the annealing experiments.

Due to a lack of suitable mineral specific or general calibrations for determining OD concentrations in spinel, the calibration of Libowitzky and Rossman [24] was also used to determine OD concentrations from normalised, integrated O–D bands. Although not specifically calibrated for OD, O–D stretching frequencies here lie well within the range of the stretching frequency-integrated molar absorption coefficient correlation upon which this calibration is based [24]. Although the error in determined O–D concentrations is likely to be higher than that of O–H concentrations, expected similarities in D and H flux (Figure 3) and diffusivities (see below) support this approach, and the effect of systematic errors in calculated OD concentrations on determination of diffusion coefficients is less significant.

Analysis of OH and OD diffusion data

Experiments were designed to produce 1-D diffusion profiles for H^+ and D^+ under experimental conditions. Cursory examination of IR line spectra is consistent with 1-D diffusion along the chosen transects, which are sufficient distance from other edges of samples to prevent any additional contributions to diffusion. As noted in Table 1, however, diffusion or H–D exchange did not occur as expected in a number of the experiments. Under the experimental conditions chosen (1 GPa, elevated temperature) H affinity in non-stoichiometric spinel is expected to be significantly enhanced prior to the onset of recrystallisation [10], thereby promoting H^+ diffusion into the spinel samples. In the case of samples annealed in D_2O, we would also expect rapid H–D exchange between the sample and surrounding capsule environment to occur, in addition to D^+ diffusion into the samples. In one sample annealed in D_2O, Hysp6, D^+ diffusion into the spinel sample was noted, evident from the presence of two additional absorption features centred around 2484 cm^{-1} (OD band 1) and 2605 cm^{-1} (OD band 2), as shown in Figure 3. These are comparable to the OH absorption bands centred around 3350 cm^{-1} and the doublet at 3520 cm^{-1} in the same sample. However, it is also apparent from the IR spectra in Figure 3 that substantial H^+ diffusion into the same sample has also occurred. This is unexpected, as it suggests that the capsule, although loaded with high-purity D_2O and sealed, also contained sufficient H^+ to act as a source for substantial H^+ diffusion into the sample. Most likely, this is due to H–D exchange with air during loading of the capsule, and then additionally between the capsule and surrounding experimental charge during the actual annealing experiment; note that the sample assembly contains talc which may provide H which can then diffuse into the central sample volume, although the presence of a thick cylinder of pyrex glass is designed to minimise this interaction. Figure 3 also shows
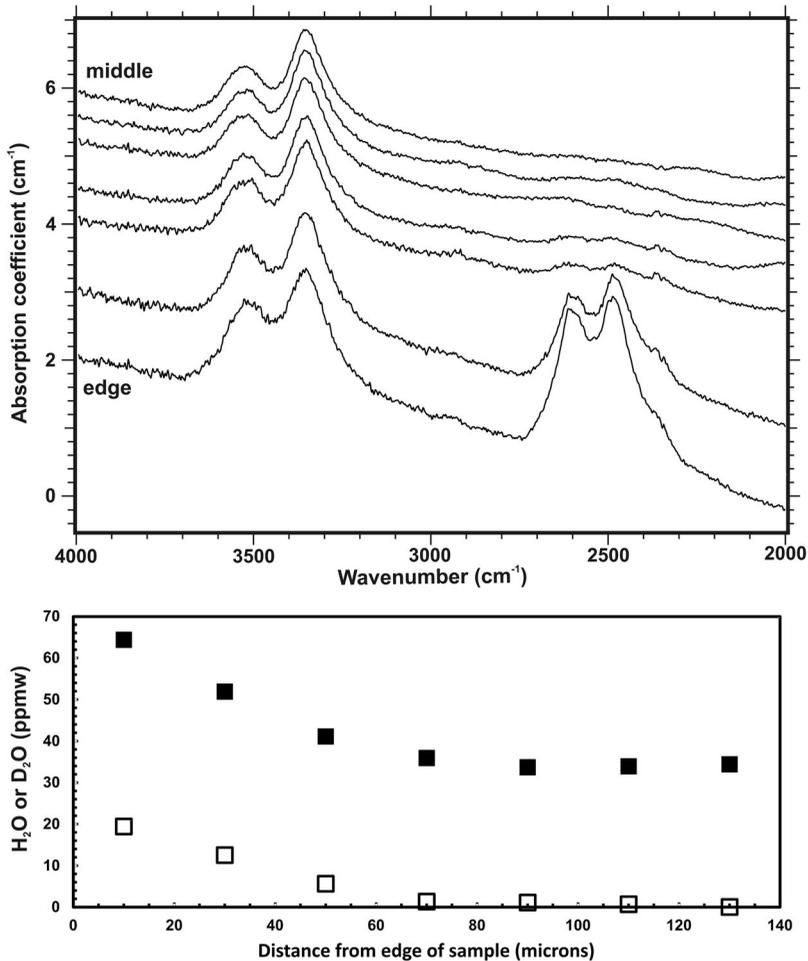
Figure 3. Top: Example of spectra from a line scan across Hysp6 6 (D_2O) showing the presence of O–H absorption bands over the region 3200–3700 cm^{-1} and the presence of corresponding O–D bands over the region 2200–2800 cm^{-1} Spectra have been thickness corrected but not background corrected, and are offset vertically for clarity, with the lowermost spectrum obtained from the edge of the annealed sample, and each overlying spectrum obtained across a line transect towards the centre of the sample, perpendicular to the edge of the sample, at progressive 20 µm steps. Bottom: Calculated total OH and OD concentrations, in ppmw H_2O (filled squares) and D_2O (open squares) from IR spectra, showing diffusion gradient for both OH and OD, implying H and D diffusion into the spinel sample rather than simple O–D isotopic exchange.

determined H_2O and D_2O concentrations across the annealed spinel sample. It is evident from the data that rates of H^+ and D^+ diffusion into the sample are comparable. Either (1) this suggests that H^+ and D^+ diffusion into the spinel is the dominant process occurring during annealing, with only limited direct H–D exchange, or (2) the kinetics of H–D exchange and H diffusion are indistinguishable. This later possibility, if correct, would imply that H^+ and D^+ diffusion into the spinel is charge balanced by flux of a faster diffusing species. This point is discussed in detail below.

Given that H and D diffusion profiles are 1-D and the result of exchange of H^+ and D^+ between the capsule environment and sample, data on H and D diffusivity, D_{eff}, can be extracted by modelling diffusion profiles using a solution to Fick's second law, assuming that the spinel and surrounding capsule act as a diffusion couple with a fixed interface (i.e. the position of the spinel crystal face, at $x = 0$), that concentration of H_2O or D_2O varies only as a function of distance into the spinel, $C(x,t)$ after annealing for time, t, that the H_2O or D_2O concentration in the 'sink' is fixed, and that the original H_2O or D_2O concentration in the spinel is C_s, such that:

$$C(x, t) = C_s - (C_s - C_0).erf\left[\frac{x}{2\sqrt{D_{eff}t}}\right] \tag{1}$$

This solution can be fitted to both scenarios encountered during annealing experiments performed here; namely: (1) H or D diffusion into the sample, where C_0 is the original H/D content in ppmw oxide, and H/D content increases due to progressive H/D diffusion from the sample edge, which has a fixed (high) concentration C_s; (2) H or D diffusion out of the sample, where C_0 is the original H/D content in ppmw oxide, and H or D loss occurs to the sample environment, with re-equilibration of H/D contents to a lower value, fixed at C_s at the sample edge. For Equation (2), it is assumed that volatile loss from capsules occurs at the onset of heating, otherwise annealing duration would be unknown, and the capsule environment variable. This assumption is discussed in more detail below. It is noteworthy that in all experiments performed here, recovered spinel cuboids showed no evidence of crystallisation or reaction with fluids or the oxide buffer used in the capsule. This is in contrast to Bromiley et al. [10] who noted considerable spinel recrystallisation. This can be attributed to (1) the lower temperatures used here for high pressure annealing, which presumably inhibit sample breakdown, and (2) the fact that the oxide buffer used here is identical in composition to the spinel crystal. EMP analysis of samples also verified that no recrystallisation or change in composition of crystals occurred during annealing experiments. Furthermore, EMP also did not reveal any gradients in Mg, Al or O towards the edge of samples, within the error of compositional analysis (standard deviations of 0.09% for Mg, 0.4% for Al and 0.7% for O). Lack of reaction between the spinel and surrounding capsule material validates the solution to Fick's second law used to determine diffusivities of H and D, which would otherwise be challenging to extract. Using this solution, all diffusion profiles were fitted to extract H or D diffusivities. Diffusivities of H and D were determined independently for D_2O diffusion experiments.

In experiments Hysp6-H_2O and Hysp5-H_2O, IR spectra reveal H^+ loss from the sample during the experiment (Figure 4), implying that the capsule failed to retain water. Data were fitted to the solution of Fick's second law to extract H^+ diffusivity and test the assumption that water was lost at the onset of the experiment (during initial heating). Similarly, in experiments Hysp5-D_2O, Hysp3-D_2O and Hysp4-D_2O, no evidence for the presence of D–O absorption bands was noted in the recovered samples, indicating loss of D_2O, supported by the presence of marked diffusion profiles demonstrating H^+ loss. Similarly, for these experiments, H diffusion profiles were also fitted to the solution of Fick's second law. Comparison with H diffusion in data could then be used to assess (1) the assumption that run failure occurs during heating, and that meaningful data on H^+ diffusivity can be extracted; and (2) to provide insight into diffusion mechanisms and defect coupling during H^+ diffusion both into and out of non-stoichiometric spinel.
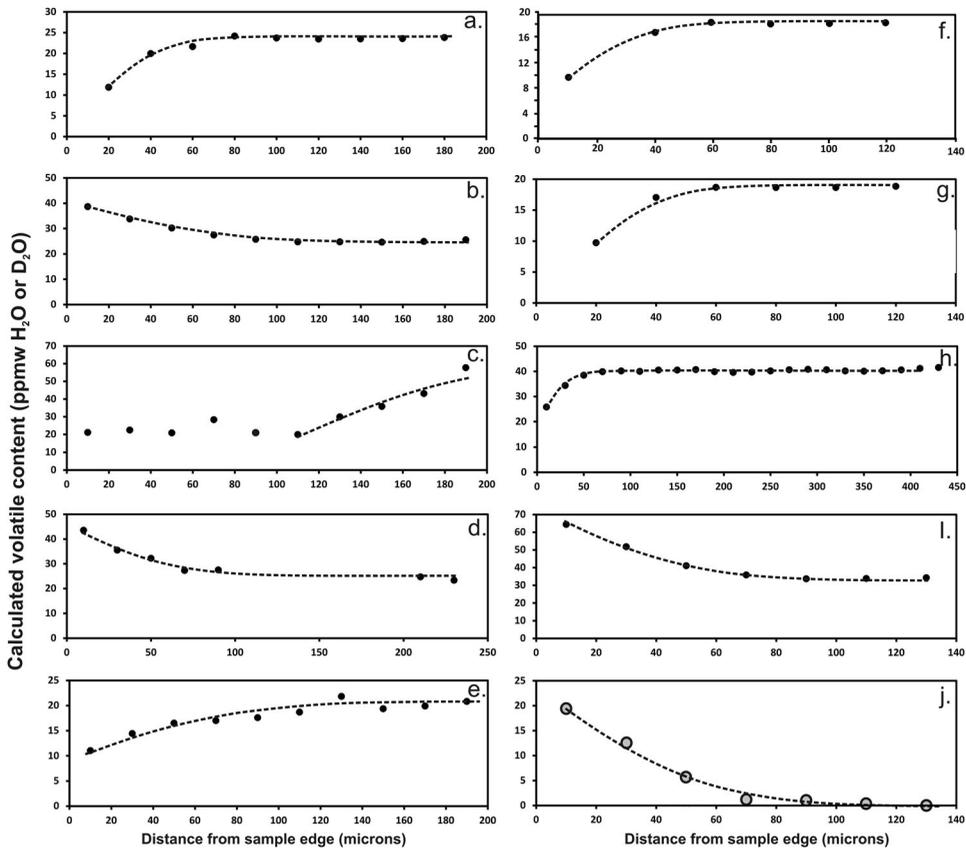
Figure 4. H and D concentration profiles in non-stoichiometric spinel, from edge to centre of samples. (a) Hysp3 (873 K, D_2O) showing H loss (no O–D detected); (b) Hysp3 (873 K, H_2O) showing H gain; (c) Hysp4 (1073 K, D_2O) showing H loss (no O–D detected); H content is uniform for the first 110 μm of the profile, presumably due to sample re-equilibration to a lower H_2O content, so only the latter part of the profile was fitted to extract H diffusivity; (d) Hysp4 (1073 K, H_2O) again showing H gain, with some data missing due to the difficulty in accurately fitting spectra with complex, non-linear baselines due to interference fringes; (e,f) two profiles from Hysp5 (773 K, H_2O) showing H loss; (g) Hysp5 (773 K, D_2O) showing H loss (no O–D detected); (h) Hysp6 (973 K, H_2O) showing H loss; (i) Hysp6 (973 K, D_2O) showing H gain; (j) Hysp6 (973 K, D_2O) also showing D gain in the same sample.

H^+ and D^+ incorporation and diffusivity in non-stoichiometric spinel

From the data it is apparent that: (1) there is some scatter in determined diffusivities, most likely due the non-uniform baselines and complex IR spectra which meant that spectra were difficult to accurately fit; (2) that there is good agreement between H^+ diffusivity determined from experiments in which H^+ diffused both into and out of spinel. In fact, there is more scatter in diffusivity data obtained from different transects across the same sample than between different samples, even between data extracted from experiments where H^+ diffused into the samples and where H^+ was lost due to run failure. This indicates that the assumption that volatiles are lost at the onset of experiments is reasonable. (3) Diffusivities for H^+ and D^+ are indistinguishable. Errors presented in Table 2 are based on the fitting procedure used, and probably significantly underestimate true

Table 2. Diffusivities for H and D in synthetic non-stoichiometric spinel at 1 GPa in both H diffusion and H–D exchange experiments.

Sample	Capsule type	Transect no.	Thickness of polished section (μm)	Process	Log D (m²/s)	10,000/T (K⁻¹)
Hysp5	H_2O	1	490	H loss (capsule failure)	−14.6 (1)	12.94
		2	490		−14.61 (2)	
Hysp3	H_2O	1	530	H gain	−14.84 (6)	11.45
		2	530		−14.31 (3)	
	D_2O	1	978	H loss (capsule failure)	−14.91 (2)	
		2	978		−14.89 (8)	
Hysp6	H_2O	1	1019	H gain	−14.5 (1)	10.28
		2	1019		−14.2 (2)	
	D_2O	1	490	H gain	−14.34 (4)	
		2	490		14.3 (1)	
		1	490	D gain	−14.3 (2)	
		2	490		14.5 (2)	
Hysp4	H_2O	1	632	H gain	−14.1 (1)	9.32
		2	632		−13.8 (8)	
	D_2O	1	489–509	H loss (capsule failure)	−13.9 (1)	

Note: Numbers in parentheses are errors on the last s.f. in quoted diffusivities.

uncertainty in diffusivities determined here. A more significant source of error is likely to arise from how spectra are fitted (as discussed above), which can result in systematic and non-systematic errors in calculated H and D concentrations. Sources of such error include: (1) non-uniform backgrounds to many of the spectra,; (2) thickness correction, which was determined optically; (3) variations in sample thickness across transects in a few samples, which had to then be additionally corrected; (4) difficulties in accurately fitting spectra with multiple contributions (*i.e.* fine structure to all absorption bands) in a consistent manner. An additional source of error in determined diffusivities could also arise from the spectroscopic technique used. A fixed aperture was used to determine OH absorption as a function of distance, ensuring that spectra were recorded from 20×20 μm areas of the top surface of the prepared samples. However, the IR beam passing through the sample is slightly conical, implying that spectra are recorded through slightly cone-shaped volumes of the sliced samples. This would result in slightly lower spatial resolution than the 20 μm aperture, and would lead to a slight overestimate of the length of diffusion profiles. This effect has not been corrected for results presented. However, to ensure that the conical sampling did not result in discrepancies in determined water contents close to the edges of sample slices, spectra were not obtained immediately adjacent to sample edges, and where possible, samples were polished to similar thicknesses to minimise systematic error. Uncertainty in determined diffusivities can be more meaningfully assessed by examining consistencies in determined diffusivities during H⁺ gain. From Figure 5, and with consideration to the fitting procedure used here, we estimate uncertainties in H⁺ and D⁺ diffusivities to be approximately ±0.3 log units, with no observed difference in diffusivity during contrasting H⁺ loss or gain. Despite these uncertainties, a temperature dependence for both H and D diffusivity can be determined:

$$D_{eff}^{H/D}(m^2/s) = 4 \pm 1 \times 10^{-12} \exp\left(-54 \pm 2 \text{kJ mol}^{-1}/RT\right) \tag{2}$$

Temperature dependence of H⁺ diffusivity is based on fitting all data. Importantly, however, within error a similar temperature dependence is noted if only data for H diffusion into non-stoichiometric spinel is used.
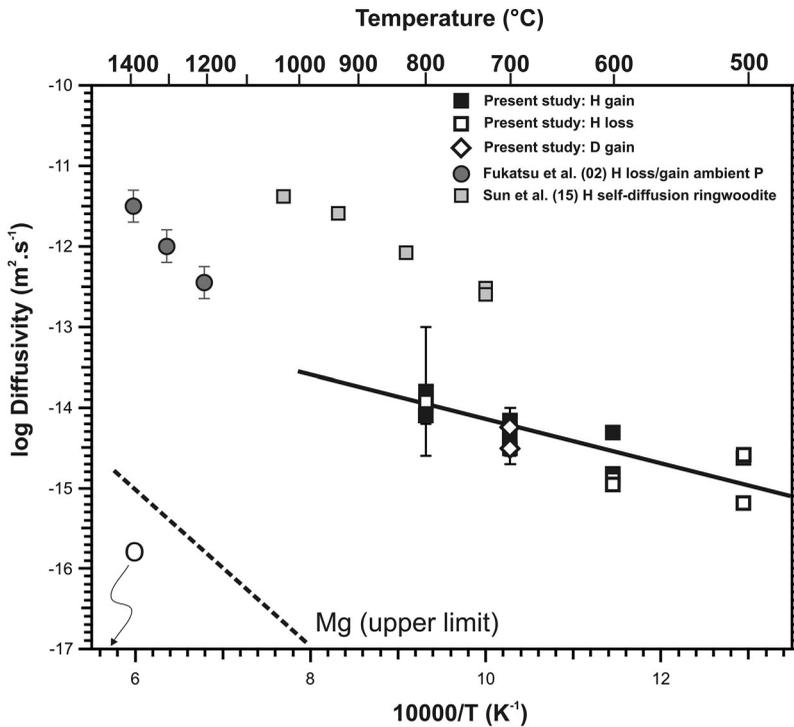
Figure 5. Arrhenius plot showing the temperature dependence of H^+ and D^+ diffusivity in non-stoichiometric spinel determined from IR analysis. Multiple data points at each temperature, where present, show the results of fitting multiple diffusion transects in both samples. Error bars on determined diffusivities and temperatures are smaller than plot size unless shown, although a more realistic error would be significantly larger, as a more significant source of error results from fitting IR data (see text for further discussion). Bold, black line is fitted Arrhenius law to all data points. Grey circles are data on H diffusion in non-stoichiometric spinel by at ambient pressure [14] and grey squares are H self-diffusion in ringwoodite from [27]. Hatched line represents likely upper limit for Mg diffusivity in non-stoichiometric spinel (see [28] for discussion; Fe-Mg exchange and Al diffusivity broadly comparable), with arrow indicating O diffusivity. As noted in [28], the observed compositional dependence of O diffusivity non-stoichiometric spinel indicates that in these studies, O diffuses via an interstitial mechanism and that as such, there is no data on O vacancy diffusion.

There are two main O–H (and corresponding O–D) absorption features in IR spectra in all samples centred around 3345–3352 and 3524–3530 cm^{-1}, assigned O–H bands 1 and 2, respectively, by Bromiley et al. [10]. Lenaz et al. [9], in a study of water incorporation in natural and synthetic spinel, assigned these bands to protonation of unshared M O–O edges ($^{VI}O–O_{unsh}$) and T O–O edges ($^{IV}O–O$), with protonation coupled with T site vacancies (V_T). However, both Gonzalez et al. [16] and Bromiley et al. [10] noted additional fine structure in O–H absorption in non-stoichiometric spinel, and a splitting of OH band 2 into at least two Gaussian contributions. Fukatsu et al. [14] suggested that O–H and corresponding O–D stretching frequencies in IR spectra were consistent with protonation of both octahedral and tetrahedral edges. On the basis of crystal structure refinements and correlation of O–H stretching frequencies with O–H … .O bond distances, Bromiley et al. [10] proposed two alternative assignments: (1) O–H band 1 due to protonation of

$^{VI}O–O_{unsh}$ and splitting of O–H band 2 due to protonation of $^{IV}O–O$ about both filled and vacant T sites; (2) band 1 due to protonation of a shared O–O M edge ($^{VI}O–O_{sh}$), band 2a due to protonation of a $^{VI}O–O_{unsh}$ and band 2b due to protonation of $^{IV}O–O$. Corresponding O–D bands in spinel in the present study are centred around 2470–2480 and 2603–2615 cm^{-1}, consistent with [16] and with previous assignments of proton positions based on O–H … O bond distances. However, higher quality IR data in the present study indicate finer structure in O–H and O–D absorption bands than previously noted, and at least four Gaussian contributions. O–H stretching frequencies are not sufficiently different to allow accurate assignment of these different contributions to specific O–O edges in the spinel structure once the effects of defect coupling are taken into consideration, especially if O–H bands are not strictly collinear with O–O edges. Fine structure in O–H and O–D absorption bands indicates protonation of at least two of the three O–O edges in the spinel structure, with additional splitting most likely to occur due to association or 'coupling' of H defects with cation vacancies and Mg–Al disorder, notably protonation about Mg'_{Al} defect centres.

As previously suggested [10,14], H$^+$ diffusion in non-stoichiometric spinel is most likely charge balanced by counter-flux of oxygen vacancies ($V_{O}^{..}$), due to the sluggish kinetics of cation diffusion at lower temperatures and observed independence of H$^+$ diffusion on formation of Mg/Al precipitates. This is consistent with observed H diffusivity in the present study, although a lack of data on $V_{O}^{..}$ diffusion in spinel makes this inference difficult to test. Importantly, there is no difference in diffusivity of H$^+$ and D$^+$ in non-stoichiometric spinel. This is consistent with absolute rate theory which predicts only a small difference between diffusivity of D$^+$ and H$^+$ due to similar mean thermal velocities. D$^+$ diffusion coupled with $V_{O}^{..}$ also explains why H$^+$ and D$^+$ diffusivities in Hysp6 are identical within error, even though D$^+$ diffusion into this sample might have occurred via both D$^+$ diffusion and, possibly, limited D$^+$–H$^+$ exchange.

Previous workers have indicated that H$^+$ incorporation in non-stoichiometric spinel can be charge balanced by Mg vacancies ($V_{Mg}^{//}$) and Al vacancies ($V_{Al}^{///}$). In particular, non-stoichiometric spinel contains high concentrations of M site vacancies, so additionally, protonation of vacancies would appear to be highly favourable due to the strong net negative charge associated with cation vacancies (i.e. associated $H_i–V_{Al}^{///}$ defects involving single or multiple protons) [10,14–16]. However, in all IR spectra here relative areas of all O–H contributions remain unchanged across diffusion profiles, during either H$^+$ loss or H$^+$ gain. Experiments were conducted at different temperatures, under which different degrees of Mg–Al ordering might be expected. Redfern et al. [17] demonstrated that localised movement of Mg and Al in stoichiometric spinel (change in the extent of ordering) occurs over timescales of tens of minutes at temperatures >900 K. Therefore, an absence of changes in relative O–H band area (and fine structure) between samples implies that either: (1) Mg–Al ordering is suppressed in non-stoichiometric spinel under these conditions [10], or (2) that Mg–Al ordering has no influence on defect association/coupling and protonation. Lack of observable changes in fine structure of O–H bands across diffusion profiles also has important implications for considering defect coupling. Fine structure of OH absorption bands can only be explained by protonation of multiple O–O edges in spinel, and association of H$^+$ with other defects. However, H$^+$ defects associated with cation vacancies or other defect centres would be expected to have a substantially reduced mobility compared to uncoupled H$^+$ (free protons) which should result in

marked changes in spectra across diffusion profiles, especially at the low temperatures used here. Lack of observed changes in fine structure of O–H absorption bands can be explained by considering temporal changes in defect association/coupling at elevated P–T. IR spectra provide insight into fine structure of O–H absorption bands due to defect coupling (*i.e.* NNN interactions) in quenched samples. In contrast, absolute determination of H_2O contents with distance may in fact provide only an assessment of bulk mobility of H^+ during annealing. During high P–T annealing, it is clear that a significant proportion of structurally bound H^+ in non-stoichiometric spinel is mobile, and able to hop from site to site (both T and M O–O edges) throughout the structure, and that H^+ mobility cannot be constrained by the mobility of other defects which give rise to fine structure in IR spectra. At any given distance, a certain proportion of H^+ may be associated with vacant cation sites, or, for example, with defects arising from Mg–Al ordering, such as octahedral sites containing Mg (Mg'_{Al}). These defects will be inherently less mobile during annealing, and for run conditions used here, can be considered immobile compared to H^+. A considerably greater activation energy would be required to mobilise H^+ associated with such defects. However, during annealing, mobile H^+ could become coupled, and then uncoupled from such defects during net diffusion through non-stoichiometric spinel structure; that is, at any given time, or at any given distance into the annealed crystal, only a proportion of the H^+ is associated with other defects. Direct evidence for such dynamic defect 'uncoupling' involving structurally incorporated H^+ has been observed in long duration annealing experiments on H-bearing diopside. Bromiley et al. [23] noted that changes in H^+ solubility in diopside and fine structure of O–H absorption bands inferred from IR spectra could only be explained by diffusion of H^+ away from substitutional defects and cation vacancies (*i.e.* defect centres) at elevated P–T. Therefore, diffusivity measurements only give an average assessment of total H^+ mobility through defect spinel, and as H^+ diffuses through the structure, it can become locally coupled and decoupled to other defects. This explanation essentially separates inferences on H^+ incorporation mechanisms and defect coupling/association from consideration of the relative mobility of defects, and is preferred because it explains both the fine structure of IR bands and the observed lack of changes in IR spectra across profiles without requiring either unrealistically fast diffusion of slow moving species, or an absence of defect coupling, both of which are counter-intuitive and unsupported by spectroscopic information. It does, however, imply that H^+ and D^+ mobility is constrained by the extent of defect association.

Comparison with previous studies, and implications for proton conduction in spinel phases

Fukatsu et al. [14] determined H^+ diffusivity in non-stoichiometric spinel similar to that studied here in a series of H uptake/loss experiments at ambient pressure and high temperature, also shown in Figure 5. They used a contrasting method to determine H^+ diffusivity, in which platelets of non-stoichiometric spinel were annealed under controlled atmospheres at ambient pressures, and observed that during their high temperature annealing experiments rapid sample recrystallisation occurred. Furthermore, they also determined H^+ diffusion on the basis of total O–H absorption through thin plates of non-stoichiometric spinel in an H_2-rich atmosphere, which, coupled with sample

recrystallisation, could indicate some additional near-surface effect which additionally contributed to O–H uptake in their samples. For example, O–H absorption onto spinel (100) surfaces annealed in H_2 has been recently shown to differ considerably from O–H bulk incorporation [22], with O–H showing a high affinity for incorporation into alumina-rich (Mg-free) surface layers. Annealing of non-stoichiometric spinel at ambient pressure and the high temperatures used by Fukatsu et al. [14] additionally promotes alumina precipitation, resulting in the penetration of reaction fronts into bulk crystals [26]. This precipitation reaction is not energetically favourable at high pressures due to the large lattice strain energy associated with alumina growth, and would be further suppressed in the present study by the lower annealing temperatures used.

Temperature dependence of H diffusivity determined by Fukatsu et al. [14] differs considerably and is inconsistent with results from the present study. This could be due to experimental issues arising from the technique they employed, or indicate an alternative mechanism for H^+ mobility at higher temperature. A change in H^+ diffusion mechanism has been proposed to explain discrepancies in studies of other NAMs. For example, Karato [19] proposed that at low temperatures used in electrical conductivity studies of olivine, movement of highly mobile free-protons dominated, compared to mobility of more complex species such as coupled protons adjacent to cation vacancies $(2H)^x_{Me}$ in diffusion experiments at higher temperature. Fukatsu et al. [14] also determined electrical conductivity in non-stoichiometric spinel, and found that measured values could not be explained by proton conduction, based on their determined H diffusivities. Instead they concluded that the dominant charge-carrying species was most likely Mg vacancies. As such, conductivity measurements and observed formation of surface oxide layers in the Fukatsu et al. [14] study might indicate an additional role of cation vacancy diffusion on H^+ mobility in non-stoichiometric spinel at high temperatures. This would be consistent with the greater temperature dependence of H^+ diffusivity at high temperature. In contrast, at low temperatures we observe no effect of cation vacancy diffusion. Figure 5 also shows H self-mobility in ringwoodite, which is isostructural with non-stoichiometric spinel, determined by Sun et al. [27] from H–D exchange experiments. Comparison suggests that H^+ mobility in ringwoodite is approximately 2 log units faster than in non-stoichiometric spinel, if it is assumed that data here provide true assessment of H mobility unconstrained from diffusion of slower moving species. However, temperature dependence of H^+ mobility in ringwoodite and non-stoichiometric spinel is broadly comparable, and markedly lower than in non-stoichiometric spinel at high temperature. Notably, Sun et al. [27] suggest that their H^+ self-mobility data are consistent with laboratory measurements of proton conductivity, although they obtained no spectroscopic data on O–H bonding environments in their samples. As such, of defect coupling during H^+ diffusion in ringwoodite cannot be assessed. Lack of changes in the fine structure of O–H absorption bands during H^+ diffusion (both H^+ gain and H^+ loss) in non-stoichiometric spinel can only be meaningfully explained by variable coupling and uncoupling of H^+ defects, where a proportion of H^+ is always coupled with other defects; this implies that application of diffusivity data to constrain proton conductivity in similar structures can only be made once the effects of defect coupling are constrained. This tentatively supports the assertion that diffusion and self-diffusion studies cannot necessarily be used to determine proton conductivity in olivine [19], and by extension other NAMs, because H^+

mobility in diffusion studies is complicated by the effects of defect coupling, in contrast to conductivity studies in which mobility of a small proportion of free protons dominates.

Acknowledgements

Disclosure statement

Funding

ORCID

Geoffrey D. Bromiley ⓘ http://orcid.org/0000-0002-2999-4235

References

[1] Bell D, Rossman G. Water in earth's mantle. The role of nominally anhydrous minerals. Science. 1992;255:1391–1397.

[2] Ingrin J, Skogby H. Hydrogen in nominally anhydrous upper-mantle minerals: concentration levels and implications. Eur J Mineral. 2000;12:543–570.

[3] Bolfan-Casanova N, Keppler H, Rubie D. Water partitioning between nominally anhydrous minerals in the MgO–SiO$_2$–H$_2$O system up to 24 GPa: implications for the distribution of water in the Earth's mantle. Earth Planet Sci Lett. 2000;182:209–221.

[4] Gaetani G, Grove T. The influence of water on melting of mantle peridotite. Contrib Mineral Petrol. 1998;131:323–346.

[5] Huang X, Xu Y, Karato S. Water content in the transition zone from electrical conductivity of wadsleyite and ringwoodite. Nature. 2005;434:746–749.

[6] Mackwell S, Kohlstedt D, Paterson M. The role of water in the deformation of olivine single crystals. J Geophys Res. 1985;90:11319–11333.

[7] Schmandt B, Jacobsen SD, Becker TW, et al. Earth's interior: dehydration melting at the top of the lower mantle. Science. 2014;344:1265–1268.

[8] Smyth J, Frost D, Nestola F, et al. Olivine hydration in the deep upper mantle: effects of temperature and silica activity. Geophys Res Lett. 2006;33:L15301.

[9] Lenaz D, Skogby H, Nestola F, et al. OH incorporation in nearly pure MgAl$_2$O$_4$ natural and synthetic spinels. Geochim Cosmochim Acta. 2008;72:475–479.

[10] Bromiley GD, Nestola F, Redfern SAT, et al. Water incorporation in synthetic and natural MgAl2O4 spinel. Geochim Cosmochim Acta. 2010;74:705–718.

[11] Kudoh Y, Kuribayashi T, Mizohata H, et al. Structure and cation disorder of hydrous ringwoodite, γ-Mg$_{1.89}$Si$_{0.97}$O$_4$. Phys Chem Miner. 2000;27(7):474–479.

[12] Pearson DG, Brenker FE, Nestola F, et al. Hydrous mantle transition zone indicated by ringwoodite included within diamond. Nature. 2014;507:221.

[13] Smyth J, Holl C, Frost D, et al. High pressure crystal chemistry of hydrous ringwoodite and water in the earth's interior. Phys Earth Planet Int. 2004;143–144:271–278.

[14] Fukatsu N, Kurita N, Shiga H, et al. Incorporation of hydrogen into magnesium aluminate spinel. Solid State Ionics. 2002;152–153:809–817.
[15] Gonzalez R, Chen Y. Transport of hydrogenic species in crystalline oxides: radiation and electric-field-enhanced diffusion. J Phys: Condens Matter. 2002;14:R1143–R1173.
[16] Gonzalez R, Chen Y, Barhorst J, et al. Protons and deuterons in stoichiometric and nonstoichiometric $MgAl_2O_4$. J Mater Res. 1987;2:77–81.
[17] Redfern S, Harrison R, O'Neill HSC, et al. Thermodynamics and kinetics of cation ordering in $MgAl_2O_4$ spinel up to 1600°C from in situ neutron diffraction. Am Miner. 1999;84:299–310.
[18] Du Frane WL, Tyburczy JA. Deuterium-hydrogen exchange in olivine: implications for point defects and electrical conductivity. Geochem Geophys Geosys. 2012;13. DOI:10.1029/2011GC003895
[19] Karato SI. Theory of isotope diffusion in a material with multiple species and its implications for hydrogen-enhanced electrical conductivity in olivine. Phys Earth Planet Int. 2013;219:49–54.
[20] Mackwell S, Kohlstedt D. Diffusion of hydrogen in olivine: implications for water in the mantle. J Geophys Res. 1990;95:5079–5088.
[21] Watson EB, Baxter EF. Diffusion in solid-earth systems. Earth Planet Sci Lett. 2007;253:307–327.
[22] Canova FF, Foster AS, Rasmussen MK, et al. Non-contact atomic force microscopy study of hydroxyl groups on the spinel $MgAl_2O_4$ (100) surface. Nanotechnology. 2012;23(32):325–703.
[23] Bromiley G, Keppler H, McCammon C, et al. Hydrogen solubility and speciation in natural, gem-quality Cr-diopside. Am Miner. 2004;89:941–949.
[24] Libowitzky E, Rossman G. An IR absorption calibration for water in minerals. Am Miner. 1997;82:1111–1115.
[25] Paterson M. The determination of hydroxyl by infrared absorption in quartz, silicate glasses and similar materials. Bull Mineral. 1982;105:20–29.
[26] Donlon WT, Mitchell TE, Heuer AH. Precipitation in non-stoichiometric spinel. J Materials Sci. 1982;17:1389–1397.
[27] Sun W, Yoshino T, Sakamoto N, et al. Hydrogen self-diffusivity in single crystal ringwoodite: implications for water content and distribution in the mantle transition zone. Geophys Res Lett. 2015;42:6582–6589.
[28] Van Orman JA, Crispin KL. Diffusion in oxides. Rev Mineral Geochem. 2010;72:757–825.